BMC Plant Biology

RESEARCH Open Access

Unveiling transfer RNA modifications of oil palm and their dynamic changes during fruit ripening

Dehai Deng[1,2†], Yichao Qin[1†], Xiuying Lin[1,3], Meng Chu[1,3], Daizhu Lv[4] and Huan Lin[1*]

Abstract

Background The oil palm (*Elaeis guineensis*) is a crucial agricultural commodity, yielding the highest oil output among oil-bearing crops. Despite its significance, productivity challenges persist due to genetic and environmental factors. This study breaks new ground by mapping tRNA modifications in oil palm, exploring their roles during fruit ripening, an area not extensively studied in non-model crops.

Results Utilizing advanced RNA mass spectrometry techniques, we identified 48 distinct tRNA modifications across 88 sites, alongside 164 genes associated with tRNA modifying enzymes. This comprehensive mapping reveals the decreasing nature of most tRNA modifications during fruit development, except for adenosine 2′-O methylation (Am). It hints at a gradual weakening of protein translation quality control and highlights a unique role for Am during fruit ripening. Additionally, lipidomic analysis tracked 674 lipids in oil palm fruits, indicating a correlation between tRNA modifications and the accumulation of specific lipids.

Conclusions This study mapped tRNA modifications in oil palm for the first time and showed the diversity of dynamic changes in tRNA modifications as the fruits develop.

Keywords tRNA modifications, Oil palm fruit development, RNA mass spectrometry, Epitranscriptome

Introduction

The oil palm (*Elaeis guineensis*) stands as the world's most productive oil-bearing crop, yielding two distinct types of oils from its fruit: palm kernel oil from the kernel and crude palm oil from the mesocarp, with the latter accounting for 90% of the oil palm's total oil output [1]. These oils are highly valued for their versatility, finding applications in both the culinary realm and various non-food industries such as cleaning, sanitation, biofuel production, and animal nutrition [2]. Commercial oil palm cultivation is predominantly concentrated in Indonesia and Malaysia, thriving in the equatorial belt, which is defined by a margin of 7° North and South of the Equator, representing 85% of the world's oil palm farming [3]. This crop occupies merely 7% of the total oil crop land yet

†Dehai Deng and Yichao Qin equally contributed co-first authors.

*Correspondence:
Huan Lin
linhuan@hainanu.edu.cn
[1]State Key Laboratory of Marine Resource Utilization in South China Sea, Hainan University, Haikou 570228, P. R. China
[2]School of Ecology and Environment, Hainan University, Haikou, P. R. China
[3]School of Life and Health Sciences, Hainan University, Haikou, P. R. China
[4]Analysis and Testing Center, Chinese Academy of Tropical Agricultural Sciences, Haikou, P.R. China

contributes to 38% of the global vegetable oil supply [4], underscoring its significance to the oil industry. Despite its high yield potential, the oil palm sector has challenges, including limited arable land, labor shortages, disease outbreaks, and environmental pressures [5]. Moreover, the actual yield of 3.8 tons per hectare per year falls well below the theoretical optimum of 18.2 tons [6, 7], highlighting a critical gap in productivity.

Efforts to enhance oil palm yields are hampered by its lengthy breeding cycle of 12–19 years, necessitating innovative strategies to improve breeding efficiency [8]. Techniques such as sourcing elite germplasm [9], engaging in various breeding methods (conventional hybrid [7], mutation [10], haploid [11], and transgenic breeding [12]), employing tissue cultures [13], DNA marker-assisted selection [14], and genome editing [15] are all adoptable methodologies aimed at overcoming these challenges. Despite integrating molecular methods into oil palm breeding programs, their impact has been limited by a lack of understanding of the plant's biology.

Significant milestones such as the publication of the first oil palm chloroplast and cytoplasmic genomes in 2012 and 2013 have laid the groundwork for advanced research [16, 17], yet the complexity of its large (~ 1.8Gb) and repetitive genome complicates assembly efforts. More accurate assemblies were achieved in 2020 and 2022 [18, 19]. The identification of quantitative trait loci (QTLs) through short sequence repeats (SSRs) and single nucleotide polymorphisms (SNPs) is enhancing our comprehension of the intricate traits of oil palm [5]. Targeted improvements in oil palm traits can be anticipated with the accumulation of novel molecular biological insights, meeting the growing demand for this versatile oil crop.

This paper focuses on oil palm's transfer (t) RNA modifications which, are rarely studied in non-model crops. The dynamic distribution of RNA modifications provides information beyond the transcriptome, within which the m^6A (N^6-methyladenosine; the full names and abbreviations of all modified nucleosides discussed were listed in the abbreviations section) in messenger RNA has been studied extensively in recent years [20–22]. tRNAs carry the majority of post-transcriptional RNA modifications, accounting for over 70% of the RNA modification types identified to date [23]. In the past, tRNA modifications were considered housekeepers, stably present in mature tRNAs. However, recent studies have shown that tRNA modifications are dynamic, subtly influencing the organism's developmental status and response to external stimuli by fine-tuning tRNA structures [24]. For example, modifications at specific positions on tRNAs, such as the wobble position 34, as well as positions 37 and 58, can be influenced by environmental factors. The cmo^5U34 on $tRNA^{Thr(UGU)}$ of *Mycobacterium bovis* is boosted by exposure to dissolved oxygen, enhancing the expression of genes rich in cognate ACG codons [25]. The t^6A37 found in mitochondrial tRNAs that decode ANN codons is sensitive to bicarbonate levels [26]. m^2A in both 23 S rRNA and tRNA of *Enterococcus faecalis* senses reactive oxygen species for translational regulation [27]. Research on tRNA modifications in plants is limited, with reports primarily focused on model organisms. Knockout experiments support that AtTRM10, AtTRM11, AtTRM82, and AtKTI12/AtELP1 are responsible for the m^1G, m^2G, m^7G, and ncm^5U modifications, respectively, in *Arabidopsis thaliana* [28]. Mutants of AtTRM11 exhibit early flowering traits, while AtELP1 mutants show narrow leaves and abnormal root development [28]. The AtELP3/ELO3 gene in *Arabidopsis* is essential for ncm^5U and mcm^5s^2U modifications, identified through the specific cleavage of tRNA mcm^5s^2U sites by zymocin [29]. The AtTAD2/AtTAD3 complex in *Arabidopsis* is the modifying enzyme for inosine modification at position 34 (I34) for multiple tRNAs. The knockout of AtTAD2/AtTAD3 is lethal [30]. Rice OsTRM13 adds Am modifications on $tRNA^{Gly(GCC)}$ which is related to salt tolerance and immune capabilities [31].

Targeting tRNA modifications could be a potential strategy for improving plant traits. To achieve this goal, it is essential to identify tRNA modification types in crops and understand their association with diverse traits, especially in non-model crops. We previously identified tRNA modifications in coconuts and suggested the role of Ar(p)64 modification in coconuts' response to salt stress [32]. This study discusses the distribution and dynamic change of tRNA modifications and their correlations with lipid profiles during oil palm fruit ripening.

Materials and methods

Materials and reagents

African oil palms (*Elaeis guineensis*, Tenera lineage) were planted in the experimental fields of Hainan University in Hainan P. R. China (20°3'N, 110°19'E). Fresh fruits were collected, frozen immediately by liquid nitrogen, and stored at − 80 °C by five groups: phase 1 (30–60 days post-pollination, DAP), phase 2 (60–100 DAP), phase 3 (100–120 DAP), phase 4 (120–140 DAP), and phase 5 (140–160 DAP) [33]. For quantitative tRNA modification and lipid composition analysis, six biological replicates were prepared using mesocarp samples of oil palm fruits at each developmental stage.

Nucleoside standards were purchased from commercial suppliers. A, U, C, G, I, m^6A, Um, m^5U, Cm, m^5C, and Gm were from Aladdin (P. R. China). m^1A, D, Ψ, $m^{2,2}G$, m^1I, and m^1G were from TRC-Canada (Canada). Am and ac^4C were from Shanghai-Yuanye (P. R. China). i^6A was from Macklin (P. R. China). m^2G was from TopScience (P. R. China). m^2A was from HoweiPharm (P. R. China). m^7G was from Sigma (USA). io^6A and ms^2m^6A

were from Biosynth (Switzerland). ms^2io^6A were from TLC Pharmaceutical Standards (Canada). Stock solutions of nucleosides (10–100 mM) were prepared in dimethyl sulfoxide and stored at − 20 ℃. For nucleoside analysis, mixed standard solutions (1 μM each) were prepared by diluting stock solutions with 0.1% formic acid in acetonitrile/water (90/10, v/v).

LC-MS-grade or HPLC-grade organic reagents used to prepare mobile phases of LC-MS were from ThermoFisher, Sigma, and TCI chemicals. Reagents for RNA extraction and gel electrophoresis were from Aladdin or Macklin. Benzonase and phosphodiesterase I were from Sigma. Alkaline phosphatase was from Takara. Sequencing grade RNase T_1 and RNase A were from ThermoFisher (Invitrogen).

Extraction of clean tRNA pools from the mesocarp of oil palm fruits

A method based on CTAB (cetyltrimethylammonium bromide) for isolating total RNA from tissues rich in lipids, previously documented [32], was applied to the oil palm fruit. Briefly, 1 g of mesocarp was instantly frozen in liquid nitrogen and ground to a fine powder. This powder was mixed with 15 mL of CTAB lysis solution (1.4 M NaCl, 0.1 M Tris-HCl pH 8.0, 50 mM EDTA pH 8.0, 2% CTAB, and 2% PVP-24000), 15 mL of phenol, and 3 mL of β-mercaptoethanol, and heated at 65°C for 10 min. Then, 16 mL of 1-bromo-3-chloropropane was added while constantly stirring, and the mixture was cooled on ice for 2 min before centrifuging at 12,000 rpm for 10 min at 4°C. The aqueous layer was extracted with acidic phenol and 1-bromo-3-chloropropane to remove proteins. For RNA precipitation, 3 M sodium acetate (pH 5.5) and ethanol were added, and the mixture was incubated at -80 °C for at least two hours. The RNA was collected by centrifugation, washed with 70% ethanol, and dried under vacuum.

The yield of total RNA was assessed using urea-polyacrylamide gel electrophoresis. Gel sections containing tRNA fractions were excised and extracted as described [34]. The purity and integrity of the extracted tRNA were confirmed by analysis on 10% urea-PAGE.

Nucleoside analysis

Total tRNA samples were processed using a previously described method, where they were first enzymatically digested by benzonase, phosphodiesterase I, and alkaline phosphatase [35]. The resulting mixture was dried and resolved with 0.1% formic acid in acetonitrile/water (90/10, v/v).

Nucleoside samples, including standard mixes and digested tRNAs (100 ng each), were analyzed using an Acquity UPLC BEH amide column (2.1 mm × 150 mm, 1.7 μm) at a flow rate of 0.1 mL/min with the following gradient: 0–11 min, 95% B; 11–35 min, 95 – 40% B; 35–40 min, 40% B; 40–40.1 min, 40–95% B; 40.1–60 min, 95% B. The mobile phases were 0.1% formic acid in water (phase A) and acetonitrile with 0.1% formic acid (phase B). The flow was then directed to either (1) a high-resolution mass spectrometer (Q Exactive, positive ESI) with an MS1 scan range of 200–950 m/z, or (2) a triple quadrupole mass spectrometer (QTRAP 6500, positive ESI) with optimized ion source settings.

Oligonucleotide analysis

As described previously [26], 5 μg of total tRNA was digested by RNase A or RNase T_1. Then, digests were analyzed by HPLC combined high-resolution mass spectrometer (Q Exactive, negative ESI). For pseudouridine mapping, 5 μg of total tRNA was combined with 30 μl of 41% ethanol/1.1 M trimethylammonium acetate solution (v/v, pH 8.6) and 5 μl of acrylonitrile. This mixture was then incubated at 70 °C for 2 h. Subsequently, the cyanoethylated tRNAs were precipitated with ethanol, dialyzed, and digested using RNase T_1. The resulting oligonucleotides were analyzed as previously described [36].

Targeted lipidomic analysis by LC-MS

The lipid extraction from oil palm fruits used a methyl tert-butyl ether (MTBE) protocol. The mesocarp was first pulverized into a fine powder with liquid nitrogen. Next, 200 μL of methanol, 20 μL of an internal standard mix, and 800 μL of MTBE were added to 1 g of the powdered sample. The mixture underwent vortexing and sonication in a 4 °C cryogenic water bath for 20 min, followed by a 30-minute rest at room temperature with 200 μL of Milli-Q water. After vortex mixing and centrifugation at 14,000 rpm for 15 min at 4 °C, the lipid-rich upper organic layer was extracted and dried using a termovap sample concentrator. The dried samples were reconstituted in 200 μL of an IPA/ACN (9:1, v/v) solvent, centrifuged again, and the clear supernatant was prepared for LC-MS analysis.

Targeted lipidomics were performed as described [37]. UPLC analysis was performed using a Nexera LC-30 A system with C18 (Phenomenex Kinetex, 2.1 × 100 mm, 2.6 μm) and HILIC (Phenomenex Luna NH2, 2.0 × 100 mm, 3 μm) columns. For the C18 column, the temperature was set at 45 °C and the flow rate at 0.35 mL/min, with a mobile phase of 70% acetonitrile with 5 mM ammonium acetate (A) and isopropanol (B). The gradient elution started at 20% B, increased to 60% over 5 min, then to 100% by 13 min, and returned to 20% by 17 min. The HILIC column operated at 40 °C and a flow rate of 0.4 mL/min, with a mobile phase of methanol/acetonitrile (1:1, v/v) with 2 mM ammonium acetate (A) and 50% acetonitrile with 2 mM ammonium acetate (B). The gradient started at 3% B, increased to 100% by

13 min, held at 100% until 17 min, and dropped back to 3% by 22 min. Samples were kept at 10 °C in the autosampler and processed in a randomized sequence to minimize instrument signal variability. Detection was carried out in both positive and negative ESI modes on a QTRAP 6500 mass spectrometer, with optimized source conditions. The quantification of lipid content was calculated using a standard curve generated by spiking representative substances into real samples.

Bioinformatic analysis

We sourced the protein sequences for tRNA-modifying enzymes via the Modomics database (https://genesilico.pl/modomics/) [23]. The annotated *Elaeis guineensis* proteome (identifier UP000504607) was downloaded from UniProt (https://www.uniprot.org). We performed a Blastp search with a 1.0×10^{-6} threshold to identify homologous genes. tRNA-modifying enzyme genes were located on *Elaeis guineensis* chromosomes using EG5 in the NCBI Genome Data Viewer (https://www.ncbi.nlm.nih.gov/genome/gdv) and the MG2C v2.1 tool (http://mg2c.iask.in/mg2c_v2.1/) [38]. WoLF PSORT (https://wolfpsort.hgc.jp/) was used to predict subcellular localizations of tRNA-modifying enzymes. Employing tRNAscan-SE 2.0 [39] alongside manual check, we identified 176 tRNAs of *Elaeis guineensis* (supplementary material). The sequence listings and raw oligonucleotide datasets (derived from RNase A or T_1 assays) underwent mapping of tRNA modifications through RNA Mod Mapper [40] and the Thermo Xcalibur Qual Browser (version 4.1). The datasets collected from the QTRAP 6500 LC-MS system were examined using SCIEX OS (version 3.3.1.43). Correlation analysis and heatmaps were built using OriginPro software (version 2021 9.8.0.200).

Results and discussions

Identification of oil palm tRNA modifications by RNA-MS

We have pioneered the identification of tRNA modifications in oil palm through RNA-MS, as delineated in Figure S1. By enzymatically digesting and dephosphorylating tRNA fractions extracted from the mesocarp of oil palm, we isolated nucleosides for analysis. These were then analyzed using high-resolution mass spectrometry (HRMS) and triple quadrupole mass spectrometry (TQMS). Oligonucleotides, produced through site-specific cleavage by RNase A or T_1, were similarly subjected to HRMS. Leveraging the precision of HRMS and the sensitivity of TQMS, we have achieved a detailed identification of tRNA modifications in oil palm for the first time.

We gathered oil palm fruits at five distinct developmental stages, with discernible differences in their physical appearance and pigmentation, as showcased in Fig. 1A and B. Total RNA, extracted in its pristine and intact form (Fig. 1C), led to the isolation of tRNA fractions through gel purification. The isolation of nucleosides was achieved using the previously mentioned HILIC method. Predominantly, we employed HRMS to identify nucleosides based on their exact mass precisely. We utilized co-eluted commercial standards to confirm isomeric

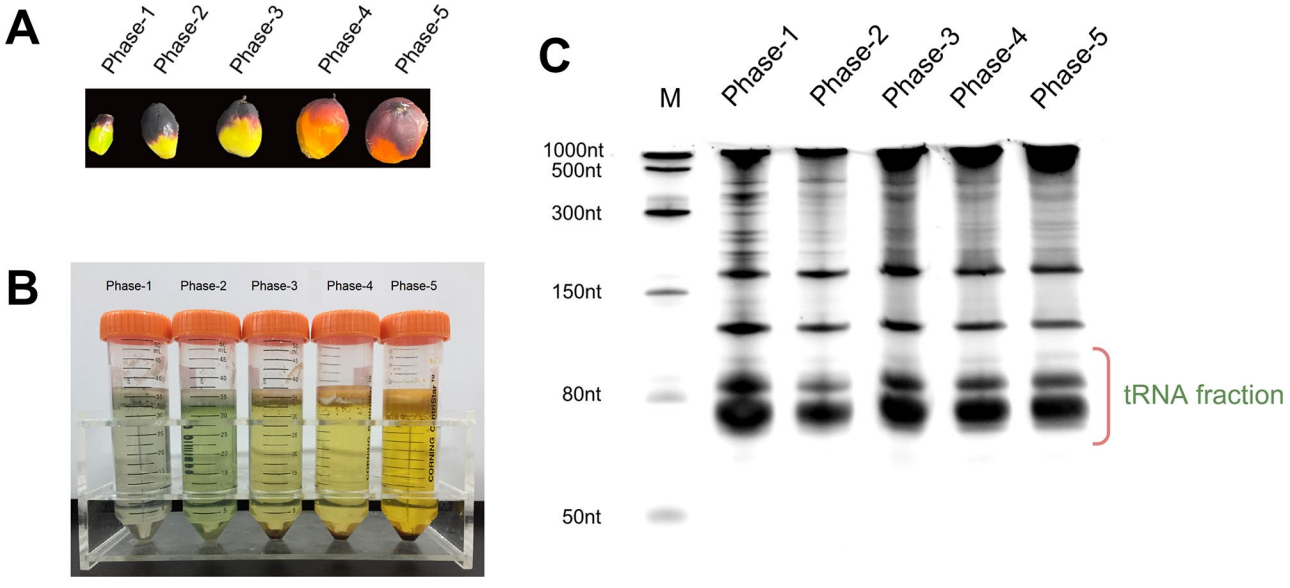

Fig. 1 Oil palm fruit and RNA extraction. (**A**) Morphological appearance of oil palm fruit at five developmental stages. Phase 1: 30–60 days post-pollination (DAP); Phase 2: 60–100 DAP; Phase 3: 100–120 DAP; Phase 4: 120–140 DAP, and phase 5: 140–160 DAP; (**B**) The lower organic phase in the RNA extraction process from the oil palm mesocarp. The color represents the pigment changes during the ripening process of oil palm fruit; (**C**) Urea-PAGE analysis of total RNA from the oil palm mesocarp across five phases. The left lane was short single-strand RNA markers. The length range of total tRNA was indicated at the bottom right

nucleosides such as m^1A, m^2A, and m^6A. Twenty-six nucleoside standards were prepared to assist qualitative analysis. HRMS enabled the identification of 29 distinct nucleosides within the tRNA fraction of the oil palm, as highlighted in Fig. 2A. With mass accuracy finer than 3 ppm, we meticulously extracted the ion chromatograms of the nucleosides (Fig. 2B). However, HRMS's sensitivity was sometimes insufficient due to positive mode ESI limitations and the low abundance of specific nucleosides. To address this, we integrated TQMS into our methodology. Leveraging the MRM mode of TQMS allowed us to detect and distinguish nucleosides by monitoring precursor (protonated nucleoside, MH^+) and product (fragmented nucleobase, BH_2^+) ions, as illustrated in Fig. 2C. This approach identified nucleosides like mnm^5s^2U and ms^2t^6A, which were elusive to HRMS (Fig. 2D). This comprehensive nucleoside analysis ultimately confirmed 35 distinct tRNA modifications in the oil palm (Table 1 and Table S1, Table S1 expands on Table 1 by adding the gene and functional annotations of homologous modifying enzymes in oil palm).

Oligonucleotide analysis allows modified RNA fragments to be ionized in negative ESI while providing position information by the CID (collision-induced dissociation) spectrum. We present an example in Fig. 3A: U[ct^6A]AGCp is a fragment digested by RNase A from

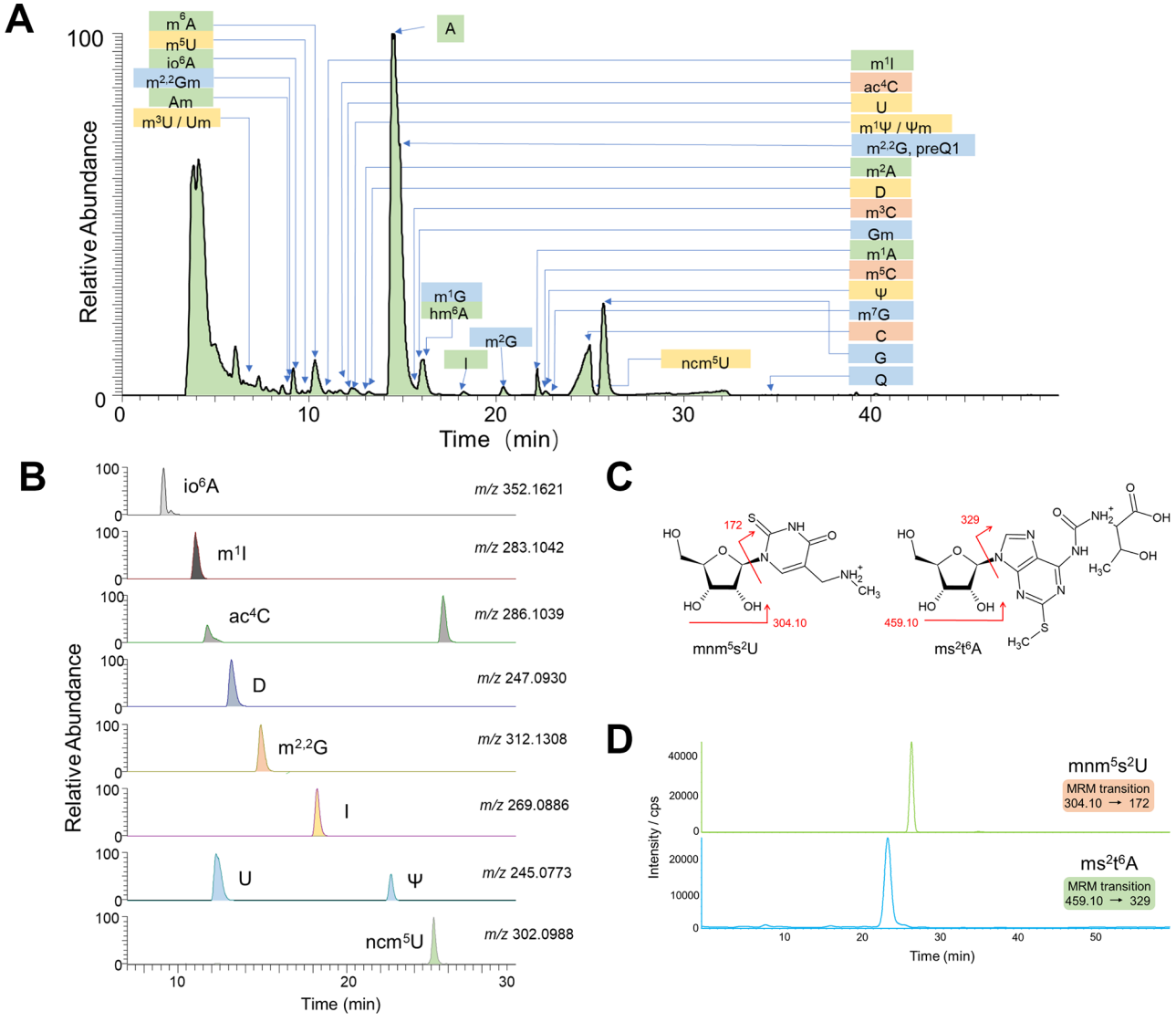

Fig. 2 Nucleoside analysis of oil palm tRNA modifications. (**A**) Total ion chromatogram (TIC) displaying the elution peaks of modified nucleosides from digested oil palm tRNAs, with arrows marking the peak positions of each nucleoside.; (**B**) Extracted ion chromatograms (XICs) for nine modified nucleosides identified in oil palm tRNA. The precise m/z value of MH^+ ion of the modified nucleoside is labeled to the right of each XIC; (**C**) Chemical structures of mnm^5s^2U and ms^2t^6A, with arrows highlighting the precursor ion (MH^+) and the product ion (BH_2^+) used for tracking these nucleosides in LC-TQMS (MRM transitions); (**d**) LC-TQMS-based detection of mnm^5s^2U and ms^2t^6A

Table 1 tRNA modifications and modifying enzymes identified by RNA-MS and homologous protein alignment in *Elaeis guineensis*

tRNA modification	m/z (z = +1)	Found in nucleoside analysis	Found in positions of oil palm tRNAs (oligonucleotide analysis)	Homologous modifying enzymes
I	269.0886	√	34	TadA (*Arabidopsis thaliana*)
				Tad1 (*Saccharomyces cerevisiae*)
m^2A	282.1202	√	37	RlmN (*Escherichia coli*)
m^6A	282.1202	√	37	TrmM (*Escherichia coli*)
ms^2m^6A	328.1079	×	37	N.D.
Am	282.1202	√	4	Trm13 (*Saccharomyces cerevisiae*)
m^1A	282.1202	√	9,15,58	Trm61 (*Saccharomyces cerevisiae*)
m^1I	283.1042	√	37	Trm5 (*Saccharomyces cerevisiae*)
m^1Im	297.1199	√	37	N.D.
i^6A	336.1672	×	37	MiaA (*Escherichia coli*)
io^6A	352.1621	√	37	MiaE (*Salmonella typhimurium*)
ms^2i^6A	382.1549	×	37	MiaB (*Escherichia coli*)
ms^2io^6A	398.1498	×	37	MiaE (*Salmonella typhimurium*)
t^6A	413.1421	×	37	TsaD (*Escherichia coli*)
ct^6A	395.1315	×	37	TcdA (*Escherichia coli*)
ms^2t^6A	459.1298	×	37*	MtaB (*Bacillus subtilis*)
Ar(p)	480.1131	×	64*	Rit1 (*Saccharomyces cerevisiae*)
Ψ	245.0773	√	2,4,5,7,8,16,27,28,31,35,38,39,41,42,45,47,47b,55	TruA (*Escherichia coli*)
				TruB (*Escherichia coli*)
				TruC (*Escherichia coli*)
				TruD (*Escherichia coli*)
D	247.093	√	16,17,20,20a,20b	Dus1/2/3/4 (*Saccharomyces cerevisiae*)
ho^5U	261.0723	√	34	TrhO (*Escherichia coli*)
				TrhP (*Escherichia coli*)
Um	259.093	√	32,39,44	TrmL (*Escherichia coli*)
m^5U	259.093	√	54	Trm2 (*Saccharomyces cerevisiae*)
ncm^5U	302.0988	√	34	AtELP1 (*Arabidopsis thaliana*)
cm^5U	303.0828	×	34	not found yet
mcm^5U	317.0985	√	34	ALKBH8 (*Homo sapiens*)
				TRM112 (*Homo sapiens*)
				Trm9 (*Saccharomyces cerevisiae*)
acp^3U	346.125	√	20,20a,20b,47	tapT (*Escherichia coli*)
$cmnm^5Um$	346.125	√	34	MnmE (*Escherichia coli*)
				MnmG (*Escherichia coli*)
mnm^5s^2U	304.0967	√	34	MnmM (*Bacillus subtilis*)
$mchm^5Um$	347.109	×	34	ALKBH8 (*Homo sapiens*)
s^2U	261.0545	×	34*	MnmA (*Escherichia coli*)
Cm	258.109	√	4,32,34	Trm7 (*Saccharomyces cerevisiae*)
				Trm13 (*Saccharomyces cerevisiae*)
s^2C	260.0705	×	32	TtcA (*Escherichia coli*)
m^3C	258.109	√	32	Trm140 (*Saccharomyces cerevisiae*)
m^5C	258.109	√	34,40,48	Trm4 (*Saccharomyces cerevisiae*)
ac^4C	286.1039	√	34	TmcA (*Escherichia coli*)
ac^4Cm	300.1195	√	34	N.D.
m^1G	298.1151	√	9,37	Trm5 (*Saccharomyces cerevisiae*)
				Trm10 (*Saccharomyces cerevisiae*)
Gm	298.1151	√	29,32,34	Trm7 (*Saccharomyces cerevisiae*)
				Trm3 (*Saccharomyces cerevisiae*)
				TrmH (*Escherichia coli*)
m^7G	298.1151	√	46,47,49	Trm8 (*Saccharomyces cerevisiae*)
m^2G	298.1151	√	4,10	Trm11 (*Saccharomyces cerevisiae*)
$m^{2,2}G$	312.1308	√	26	Trm1 (*Saccharomyces cerevisiae*)

Table 1 (continued)

tRNA modification	m/z (z = + 1)	Found in nucleoside analysis	Found in positions of oil palm tRNAs (oligonucleotide analysis)	Homologous modifying enzymes
imG-14	322.1151	×	37	TYW1 (*Saccharomyces cerevisiae*)
yW-86	423.1628	×	37*	TYW2/3/4 (*Saccharomyces cerevisiae*)
yW-72	437.1784			
yW-58	451.1941			
yW	509.1996		37	
OHyW	525.1945	√	37	hTYW5 (*Homo sapiens*)
preQ1 / Q	312.1308/410.1675	√	34*	QTRT1/2 (*Homo sapiens*)

Note: An asterisk indicates that the modification was not detected in RNA-MS, but the homologous gene of its modifying enzymes could be found

$tRNA^{Arg1(CCU)}$. This fragment was identified in MS1 (Fig. 3B), and the modification site of ct^6A was located through the CID spectrum (Fig. 3C). In this work, we mainly utilized information from c, y, and d-H_2O fragments for identification [41]. Additional eight species of tRNA modification, including s^2C, $mchm^5Um$, cm^5U, ct^6A, imG-14, yW, ms^2i^6A, and t^6A, were found by oligonucleotide analysis. Using the 176 tRNAs extracted by tRNAscan-SE 2.0 as a template, 86 distinct modification sites were confirmed in total tRNA digests. Pseudouridine (Ψ), due to its identical molecular weight to uridine, cannot be distinguished by RNA-MS. Therefore, we employed N^1-cyanoethylation to label Ψ, which resulted in a unique + 53 mass shift detectable in RNA-MS [42]. By identifying unique fragments containing Ψ within these 176 tRNAs (only fragments unique to a specific tRNA were used to mark Ψ sites), we have mapped 21 Ψ sites in oil palm tRNA (Table 2).

Mapping of tRNA modifications in *Elaeis guineensis*

While RNA-MS rigorously investigated modifications in the total tRNA of the oil palm mesocarp, it is plausible that certain modifications either do not occur in the mesocarp or exist in such low quantities as intermediate states between two known modifications, rendering them undetectable. For example, although we identified imG-14 and yW, intermediate forms like yW-86, yW-72, and yW-58 eluded detection. To uncover additional potential tRNA modifications in oil palm, we cross-referenced tRNA modification enzymes from the modomics database with the oil palm genome, discovering 164 homologous tRNA modification enzyme genes. This alignment hints at the possible existence of modifications such as s^2U34, yW-86 (37), yW-72 (37), yW-58 (37), and Ar(p)64, which RNA-MS did not identify (Table 1).

Combining all the analyses presented, we have created a comprehensive landscape of tRNA modifications in oil palm (Fig. 4). This represents the first-ever endeavor to identify and map tRNA modifications within this non-model but significant crop. Delving deeper into tRNA modifications could potentially contribute to crop traits improvement, much like manipulation of certain mRNA modifications have been shown to enhance crop yields and increase drought tolerance [43, 44].

Locations of candidate tRNA-modifying enzyme genes on oil palm chromosomes

The chromosomal locations of homologous tRNA-modifying enzyme genes in oil palm are depicted in Fig. 5. Due to the incomplete nature of the oil palm genome data, with some sequences not assembled into chromosomes, only 79 out of 164 predicted tRNA-modifying enzyme genes could be mapped to chromosomes. Chromosomal distribution models show that specific chromosomes and regions have a higher concentration of these genes. For example, Chromosomes 5, 6, 10, 13, and 16 contain only one or two tRNA-modifying enzyme genes. Chromosome 1 is the most frequent site for these genes. Unlike the coconut [32], which belongs to palmae as oil palm, the A, U, and G modifying enzyme genes in oil palm are more evenly distributed across the chromosomes. There are at least ten isoforms of enzymes modifying I, i^6A, Ψ, and acp^3U, with the genes responsible for Ψ modification distributed across nine distinct chromosomes. Predictions by WoLF PSORT indicate that their translation products are widely located in the cytoplasm and organelles (Table 1), underscoring their critical role in the growth and development of oil palm. Understanding the chromosomal distribution of tRNA-modifying enzyme genes will help study the impact of active and open chromosomal regions on tRNA modifications.

Dynamic changes of tRNA modification during oil palm fruit ripening

We tracked the changes of 24 tRNA modifications during the development of oil palm fruits using LC-TQMS. The relative abundance of each modification was represented by the intensity ratio of the four unmodified nucleosides A, U, C, and G, and each data point was normalized on a scale from 0 to 1 (Fig. 6). As shown in Fig. 6A, most tRNA modifications were expressed at certain levels during Phases 1–3, drop to lower levels in Phase 4, and

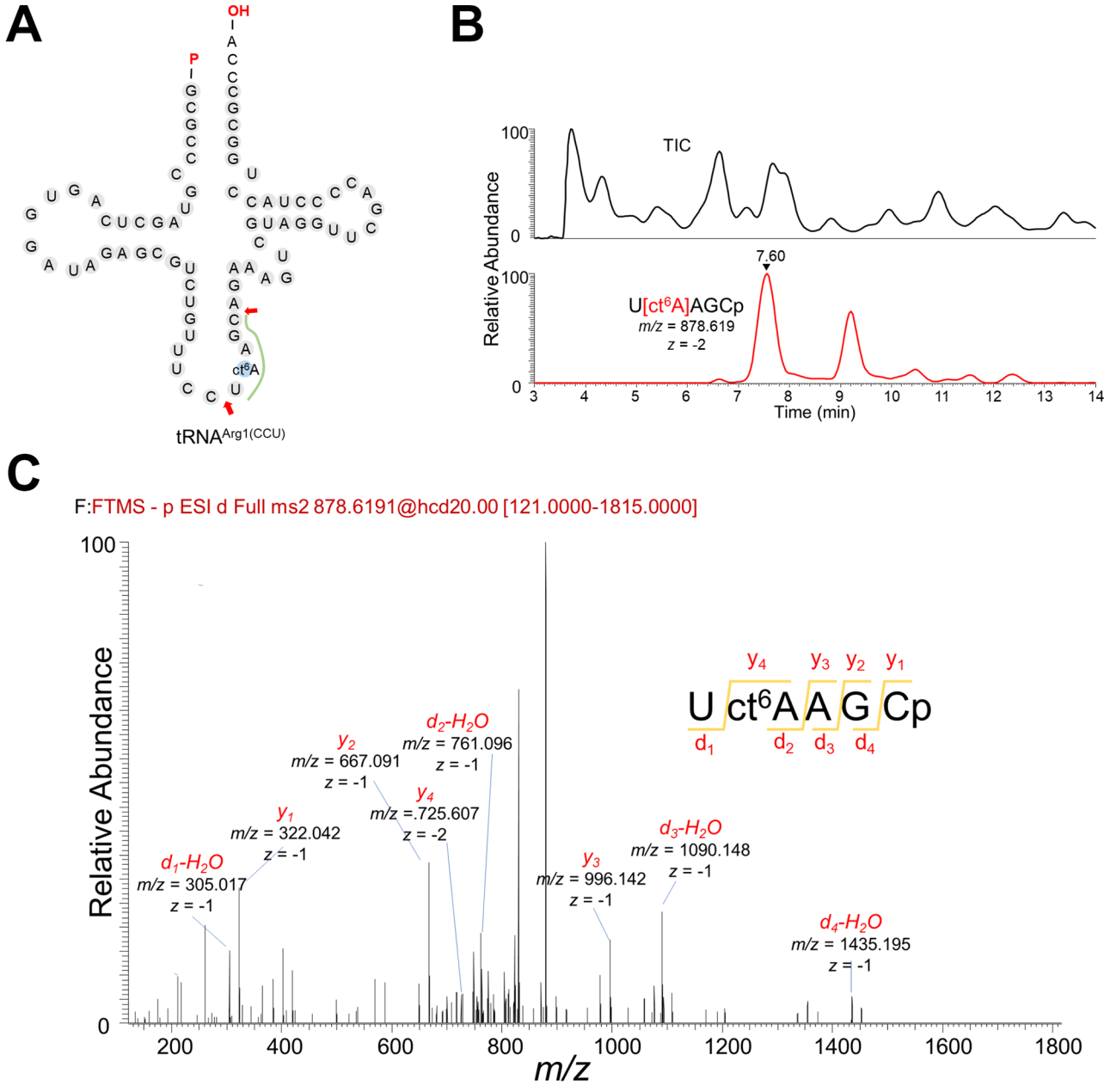

Fig. 3 Oligonucleotide analysis exemplified in oil palm tRNA. (**A**) Secondary structure of oil palm tRNA$^{Arg1\ (CCU)}$, with arrows indicating RNA fragments containing ct^{6}A37 post-RNase A digestion; (**B**) TIC and XIC of U[ct^{6}A]AGCp in oligonucleotide analysis (MS1); (**C**) CID spectrum of U[ct^{6}A]AGCp and identification of modification sites via y and d-H_2O fragments

then slightly increased in Phase 5. Since tRNA modifications are key components for ensuring tRNA function, this indicates that during Phases 1–3, the development of the fruit still required a good level of protein expression. However, as it enters Phase 4, when the fruit matures, and more energy is converted into fats, protein translation became less important, reducing quality control levels. This is reflected in the decreased levels of tRNA modifications while the overall tRNA did not degrade (Fig. 1C). In Phase 5, the resurgence of tRNA modifications suggests that protein translation is mildly reactivated in the final stages of fruit maturation. However, there is still a significant decrease in tRNA modifications in the later stages of fruit development compared to the earlier stages.

There are two notable exceptions: inosine (I) and Am. Inosine remains consistently expressed throughout the various stages of fruit development (Fig. 6A and C), whereas the level of Am experiences a dramatic increase in Phase 5, reaching approximately 15 times beyond its initial level in Phase 1 (Fig. 6B and C). In our identification work above, we found inosine exclusively at position

Table 2 Unique fragments for positioning pseudouridines and inosines in specific tRNAs

Position	Found in tRNAs	Detected Unique Fragments	Co-Positioning	MS1	MS2
2	Asp1_GUC, Asp2_GUC	[Ψ-CE]C[m^2G]UUGp	m^2G4	*m/z* = 998.123, *z*=-2	√
4	Cys4_GCA	[Ψ-CE]CCUUA[m^2G]p	m^2G10	*m/z* = 1142.646, *z*=-2	√
5	Lys1_UUU, Lys2_UUU, Lys3_UUU	[Ψ-CE]CUUA[m^2G]p	m^2G10	*m/z* = 990.126, *z*=-2	√
7	Ile1_AAU, Ile2_AAU	CCUA[Ψ-CE]UA[m^2G]p	m^2G10	*m/z* = 1307.172, *z*=-2	√
7	Tyr1_GUA	ACC[Ψ-CE]UA[m^2G]p	m^2A10	*m/z* = 1154.160, *z*=-2	√
7	Tyr1_GUA	ACC[Ψ-CE]U[m^1A]Gp	m^1G9	*m/z* = 1154.160, *z*=-2	√
8	Tyr1_GUA	ACCU[Ψ-CE]A[m^2G]p	m^2G10	*m/z* = 1154.160, *z*=-2	√
8	Tyr1_GUA	ACCU[Ψ-CE][m^1A]Gp	m^1A9	*m/z* = 1154.160, *z*=-2	√
16	Asn8_GUU	CUCA[m^1A][Ψ-CE]Gp	m^1A15	*m/z* = 1154.160, *z*=-2	√
25	Ile1_UAU, Ile2_UAU, Ile5_UAU	C[$m^{2,2}$G][Ψ-CE]UGp	$m^{2,2}$G26	*m/z* = 852.118, *z*=-2	√
27	Leu2_CAG, Phe1_GAA, Phe2_GAA, Thr1_UGU, Thr2_UGU, Thr3_UGU, Thr5_UGU	C[$m^{2,2}$G][Ψ-CE]CAG	$m^{2,2}$G26	*m/z* = 1016.152, *z*=-2	√
27	Ile1_UAU, Ile2_UAU, Ile5_UAU	C[m^2G][Ψ-CE]U[Gm]Gp	m^2G27, Gm29	*m/z* = 1024.642, *z*=-2	√
27	Val1_UAC, Val3_UAC	U[D]AUCAC[$m^{2,2}$G][Ψ-CE]UAGp	D20, $m^{2,2}$G26	*m/z* = 1305.172, *z*=-3	√
28	Arg1_ACG, Arg2_ACG	C[$m^{2,2}$G]C[Ψ-CE][Gm]G	$m^{2,2}$G26, Gm29	*m/z* = 1031.158, *z*=-2	√
33	Gln1_UUG, Gln2_UUG, Gln3_UUG, Gln4_UUG, Gln5_UUG, Gln6_UUG	AC[Ψ-CE][ho^5U]UGp	ho^5U34	*m/z* = 991.141, *z*=-2	√
33	Leu1_CAG, Leu2_CAG	U[Um][Ψ-CE]CAG	Um32	*m/z* = 990.126, *z*=-2	√
34	Ser1_AGA, Ser2_AGA, Ser3_AGA, Ser4_AGA, Ser5_AGA, Ser6_AGA	A[m^3C]U[I-CE]G	m^3C32	*m/z* = 849.119, *z*=-2	√
33	Gln1_CUG, Gln2_CUG, Gln3_CUG, Gln4_CUG, Gln5_CUG	A[m^3C][Ψ-CE]CUGp	m^3C32	*m/z* = 989.634, *z*=-2	√
35	Gln1_CUG, Gln2_CUG, Gln3_CUG, Gln4_CUG, Gln5_CUG	A[m^3C]UC[Ψ-CE]Gp	m^3C32	*m/z* = 989.634, *z*=-2	√
38	Ala4_UGC	CA[Ψ-CE][m^1G]UGp	m^1G39	*m/z* = 1009.637, *z*=-2	√
38	Ala1_AGC, Ala1_CGC, Ala2_CGC, Ala3_CGC, Ala5_CGC	C[m^1I][Ψ-CE][m^1G]CGp	m^1I37, m^1G39	*m/z* = 1016.644, *z*=-2	√
38	Pro_AGG, Pro_CGG, Pro1_UGG, Pro3_UGG, Pro4_UGG	[Ψ-CE][m^1G][m^5C]GAGp	m^1G39, m^5C40	*m/z* = 1036.156, *z*=-2	√
38	Val_GAC	AC[m^1G][Ψ-CE][m^1G]Gp	m^1G37, m^1G39	*m/z* = 1036.156, *z*=-2	√
39	Ser1_AGA, Ser2_AGA, Ser3_AGA, Ser4_AGA, Ser6_AGA	A[io^6A]A[Ψ-CE]CAUGp	io^6A37	*m/z* = 1365.712, *z*=-2	√
39	Thr4_UGU, Thr4_UGU	U[m^1Im]A[Ψ-CE]Gp	m^1Im37	*m/z* = 856.616, *z*=-2	√
40	Ser1_GCU, Ser2_GCU, Ser3_GCU	[Ψ-CE]ACA[Um]Gp	Um44	*m/z* = 1001.639, *z*=-2	√
41	Pro2_UGG	[ms^2m^6A]AAC[Ψ-CE]Gp	ms^2m^6A37	*m/z* = 1036.152, *z*=-2	√
45	Arg3_ACG	[Ψ-CE][m^7G]UC[m^7G]Gp	m^7G46, m^7G49	*m/z* = 1024.642, *z*=-2	√
47	Ala1 _AGC, Ala2 _AGC, Ala1_CGC	[m^7G][Ψ-CE]A[Cm]GGp	m^7G46, Cm49	*m/z* = 1036.156, *z*=-2	√
47	Ile2_AAU	[Ψ-CE][m^5C][m^7G]CAGp	m^5C48, m^7G49	*m/z* = 1016.152, *z*=-2	√
47b	Leu2_AAG	[m^7G][m^7G]C[Ψ-CE]UGp	m^7G46, m^7G47	*m/z* = 1024.642, *z*=-2	√
50	Arg1_CCU, Arg2_CCU, Asn8_GUU, Asn9_GUU, Trp2_CCA, Trp3_CCA	U[m^5C][m^7G][Ψ-CE]AGp	m^7G47, m^5C48	*m/z* = 1016.639, *z*=-2	√
58	Leu2_AAG	[Ψ-CE][m^2G]CU[Gm]Gp	m^2G26, Gm29	*m/z* = 1024.642, *z*=-2	√

34 of tRNAs. I34 is a significant tRNA modification produced by tRNA-adenosine deaminases, predominantly found in tRNAs whose anticodons start with an A, including $tRNA^{Arg(ACG)}$, $tRNA^{Ala(AGC)}$, $tRNA^{Ile(AAU)}$, $tRNA^{Leu(AAG)}$, $tRNA^{Pro(AGG)}$, $tRNA^{Ser(AGA)}$, $tRNA^{Thr(AGU)}$, and $tRNA^{Val(AAC)}$ [45]. The modification of A34 to I34 allows the first base of the anticodon, originally pairing only with U, to pair with A, C, and U, significantly expanding the decoding capacity of the tRNA [45]. The stable expression of I34 during fruit development suggests that it plays a housekeeper role in maintaining baseline levels of protein translation. Our data supports that Am is positioned at the fourth nucleotide of tRNAs, consistent with the widely accepted notion of Am4's conserved presence in eukaryotic tRNAs. Am4 is catalyzed by Trm13, an enzyme for which oil palm has two homologous genes (Table 1). Located within the acceptor stem of tRNAs, the precise role of Am4 remains elusive. In yeast, the deletion of Trm13 results in the loss of Am4 without causing noticeable phenotypic alterations [46]. Knockout experiments of Trm13 in rice imply a connection between Am and salt stress [31]. The pronounced increase of Am4 during the late stages of oil palm fruit development could offer valuable insights into Am4's functionality. Regardless, the distinct trends in changes of I and Am compared to other tRNA modifications may reveal their critical roles in the development of oil palm fruits.

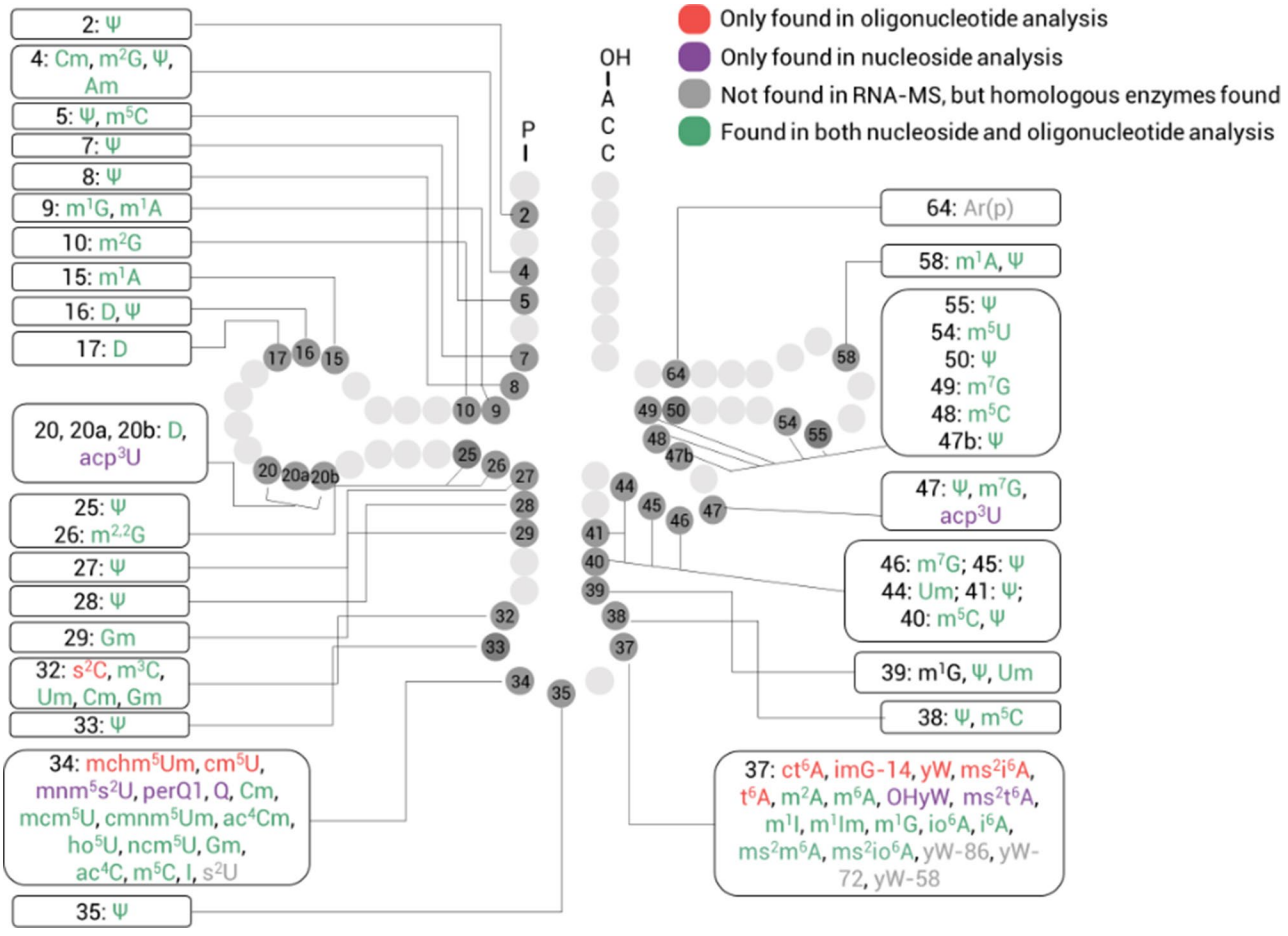

Fig. 4 Mapping of tRNA modifications in oil palm. The top right corner features a legend with different colored tRNA modifications, indicating their detection status in RNA-MS analysis: modified nucleosides marked in red were found only in the oligonucleotide analysis; modified nucleosides marked in purple were found only in the nucleoside analysis; nucleosides marked in gray were not detected in RNA-MS, but genes for their modifying homologous enzymes exist in the African oil palm genome; modified nucleosides marked in green were detected in both the oligonucleotide and nucleoside analyses. The lines and boxes mark the detected nucleosides and their positions on the tRNA

Lipid profiles of development stages of oil palm fruit

We conducted a targeted quantitative analysis of the lipid components in oil palm fruits across five developmental stages to explore their association with tRNA modifications. We identified 20 classes comprising 674 lipids, among which triglycerides (TGs; the full names and abbreviations of all lipids discussed were listed in the abbreviations section) were the most abundant, totaling 350 types (Figure S2). As depicted in Fig. 7A, there was a marked surge in the total lipid content of oil palm fruit during Phase 3, which then maintained consistently high levels through Phases 3 to 5. In terms of lipid composition, a noteworthy transformation of fatty acids (FAs) into TGs was observed in Phase 3 (Figure S3). This suggests that Phase 3 represents a pivotal juncture for the maturation of the fruit and the accumulation of oils. Examining the lipid carbon chain lengths revealed a predominant accumulation of FAs with 14 to 18 carbons, diglycerides (DGs) with 32 to 36 carbons, and TGs with 48 to 54 carbons from Phase 3 to 5 (Figure S4). Concerning carbon chain saturation, the oil palm fruit predominantly accumulated FAs with 0 to 2 double bonds, DGs with 0 to 3 double bonds, and TGs with 0 to 4 double bonds (Figure S5), indicating an overall high saturation level. The quantitative shifts in other lipid classes are depicted in Fig. 7B and C. Given the substantial variance in lipid concentrations, we normalized these trends for clearer visualization (Fig. 7D). Beyond the more abundant lipids, such as FAs, DGs, and TGs, there was a significant uptick in the levels of Cers, ChEs, PGs, MGs, and DHCers as the fruit matured. Conversely, the concentrations of Hex1Cers and SMs remained stable. This selective accumulation of lipids was observed in oil palm fruit.

Correlation analysis between lipidomics and tRNA modification dynamics

We unearthed intriguing insights through a correlation analysis between 24 tRNA modifications and absolute

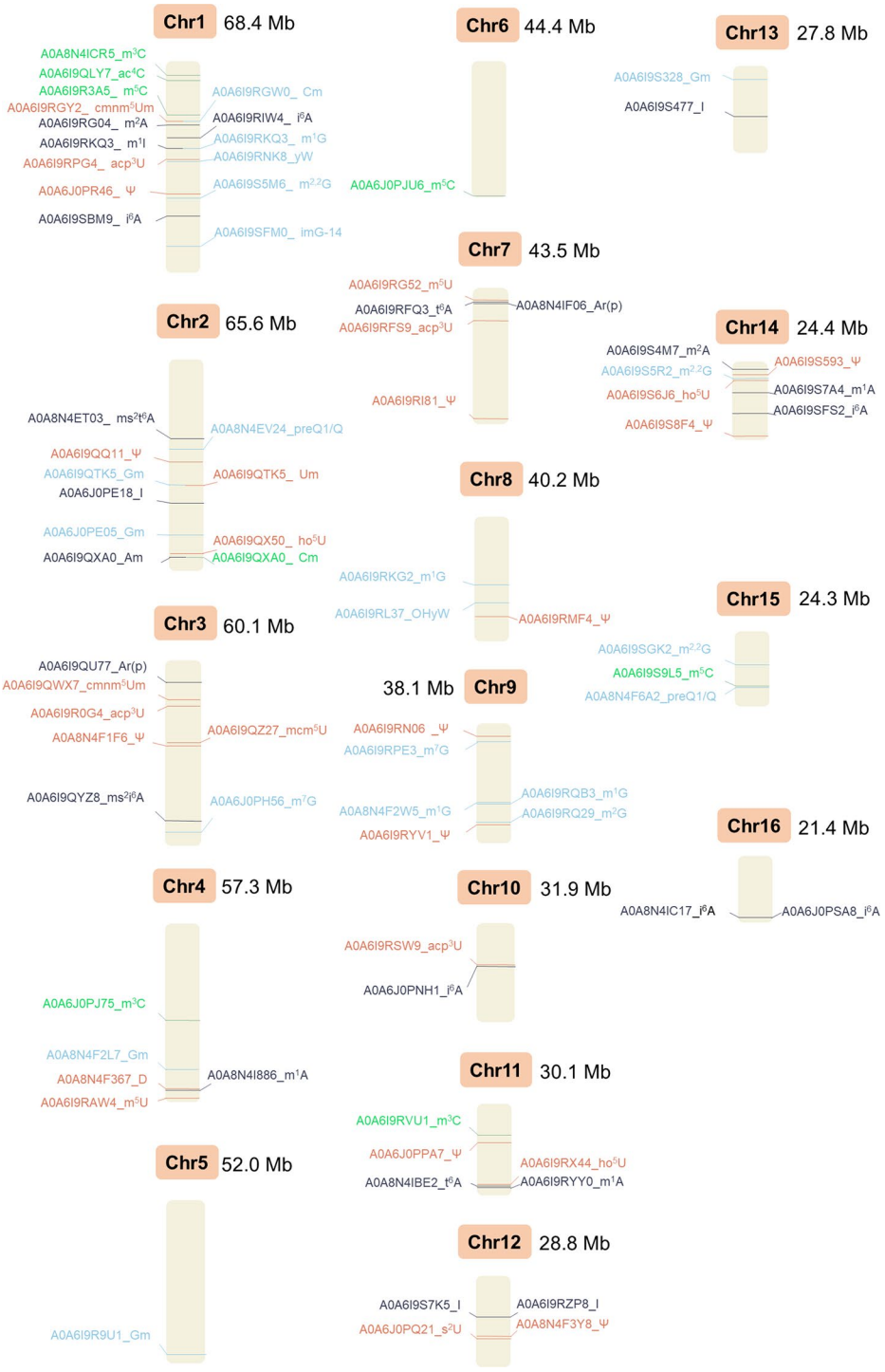

Fig. 5 The chromosomal location of the tRNA-modifying enzyme candidate genes of the African oil palm. Modifications on adenosine (**A**), uridine (**U**), cytidine (**C**), and guanosine (**G**) were distinguished with colors: black for A, brown for U, green for C, blue for G

lipid quantities (Fig. 8A) or compositional ratios (Fig. 8B). Figure 8A reveals that tRNA modifications tend to negatively correlate with the total absolute lipid content, with the notable exception of Am, which positively correlates with the quantities of most lipids. This hints at the specific role of Am in the process of lipid accumulation. Specific lipids, such as FA, LPG, PI, and PS, exhibit strong negative correlations with tRNA modifications, whereas ChE, Hex1Cer, and LPI display positive correlations with most tRNA modifications. On the other hand, LPA and LPE show little to no correlation with tRNA modifications. Intriguingly, ms^2io^6A and Am exhibited opposite

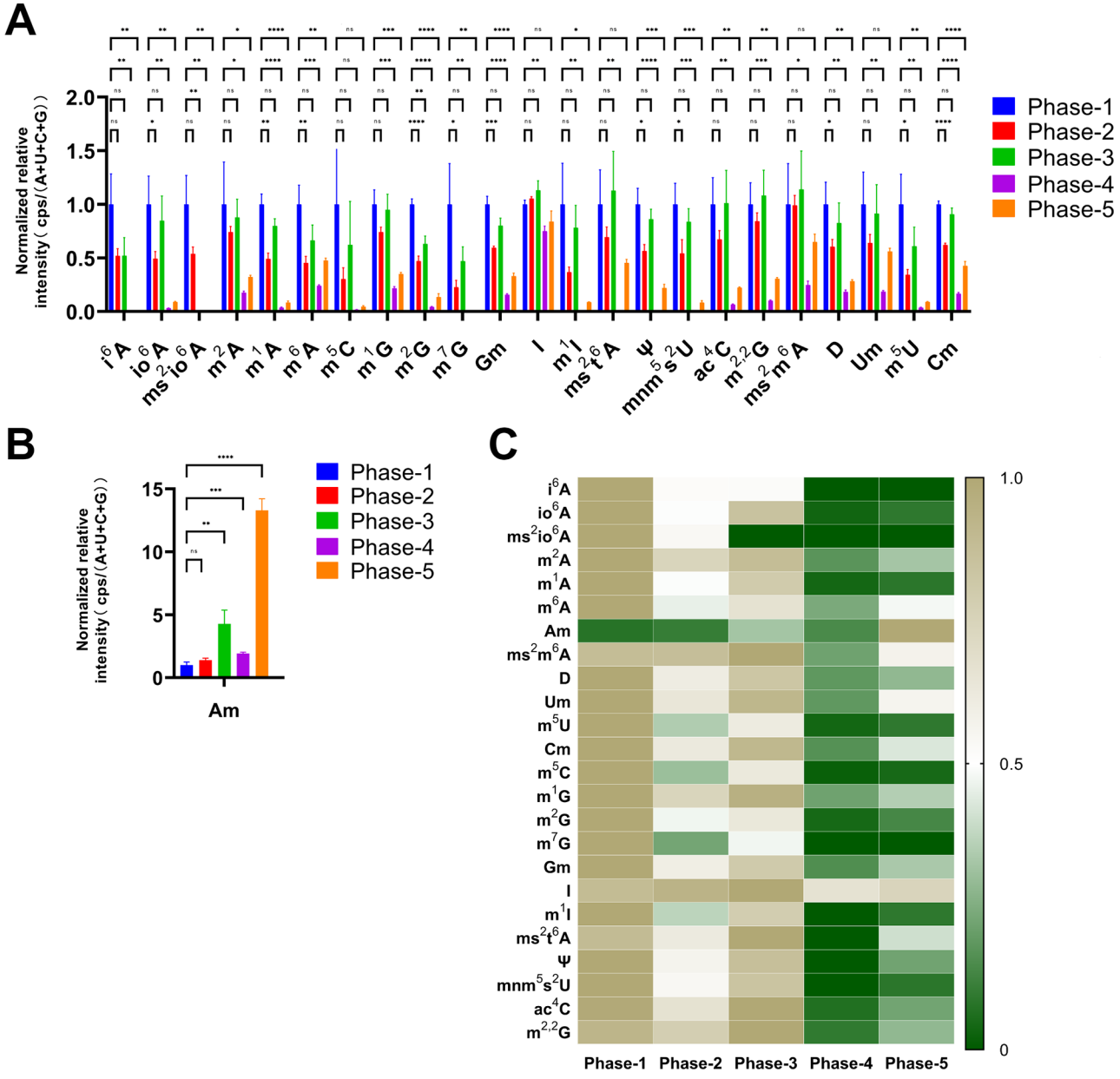

Fig. 6 Dynamic changes in tRNA modifications during oil palm fruit development. (**A**) Variation of 23 tRNA modifications across Phases 1–5, represented by the ratio of their signal intensity to the sum signal intensities of the four unmodified nucleosides AUCG. Data were normalized due to differing signal responses among nucleosides. The significance of the differences of each nucleoside between Phase 2–5 and Phase 1 is labeled, where * represents $p < 0.05$, ** represents $p < 0.01$, *** represents $p < 0.001$, and **** represents $p < 0.0001$; (**B**) Variation of Am across Phases 1–5. The significance of the differences is marked as above; (**C**) Heatmap illustrating the shifts in tRNA modifications throughout Phases 1–5. The relative content of each nucleotide was normalized to a range of 0–1

correlations with lipid accumulation. ms^2io^6A, which can arise as a free monomer from tRNA degradation, is part of the cytokinin family, known explicitly as 2-methylthio-cis-Zeatin riboside (ms2cZR) [47]. Its primary association with promoting plant growth rather than energy storage provides a plausible explanation for its negative correlation with lipid accumulation. When the focus shifts to lipids' compositional ratios (relative content) in Fig. 8B, most tRNA modifications positively correlate with lipids, except for Am, which negatively correlates with them. Am is only positively correlated with the relative content of TGs, while the effect of ms^2io^6A remains the exact opposite. The compositional ratio of FAs is negatively correlated or uncorrelated with most tRNA modifications, except ms^2io^6A. Despite an overall increase in lipid content, the changes in the proportional structure of various lipid classes still show a certain association with tRNA modifications.

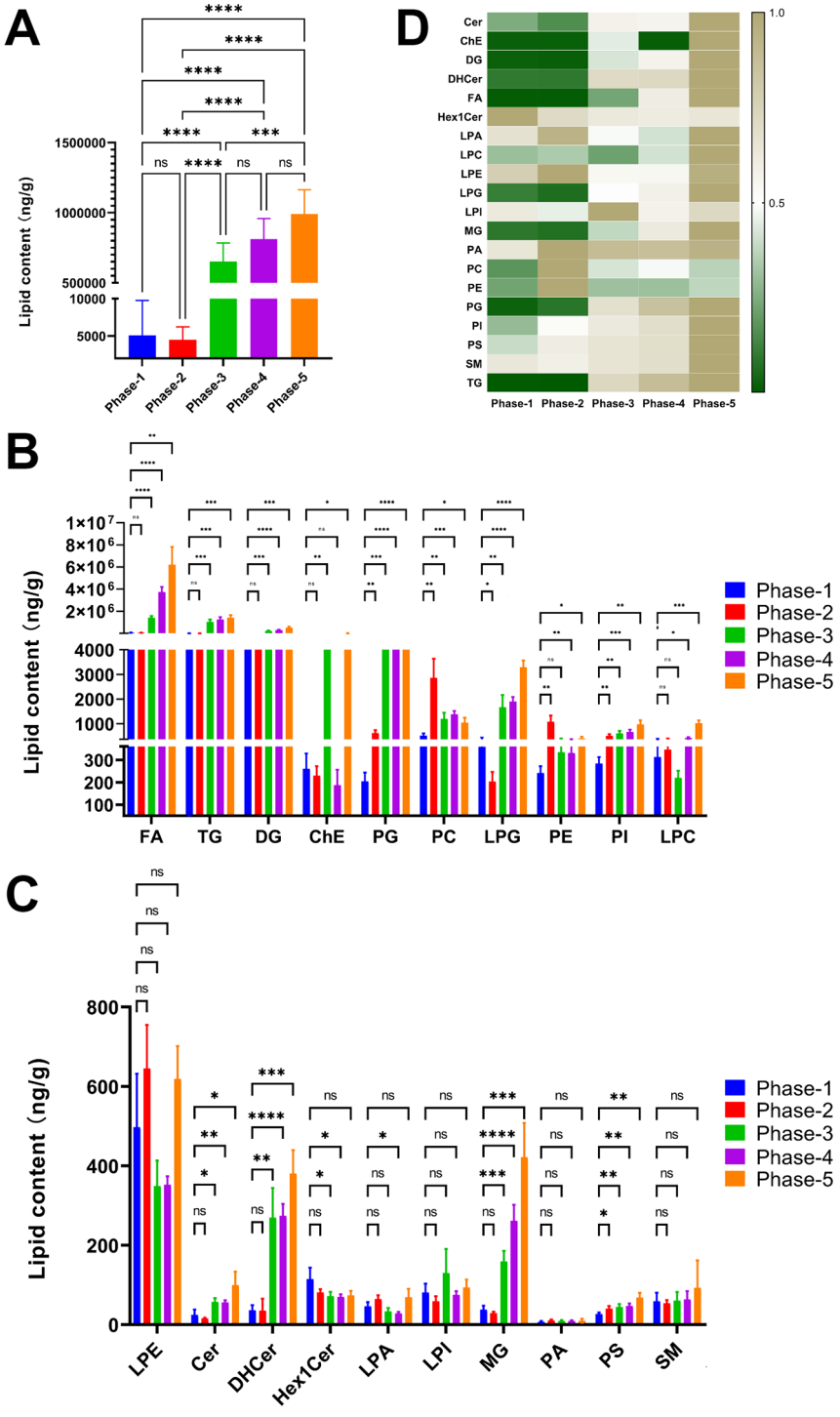

Fig. 7 Changes in the lipid profile during oil palm fruit development. The unit for lipid content is nanogram per gram of fresh weight of the oil palm mesocarp (ng/g). (**A**) Variation in total lipid content across Phases 1–5. The significance of the differences is labeled, where * represents $p < 0.05$, ** represents $p < 0.01$, *** represents $p < 0.001$, and **** represents $p < 0.0001$; (**B**) Changes in the content of 10 lipid classes throughout Phases 1–5 (FA and others). The significance of the differences is labeled as above; (**C**) Changes in the content of 10 lipid classes across Phases 1–5 (LPE and others). The significance of the differences is labeled as above; (**D**) Normalized (0–1) heatmap of 20 lipid classes over Phases 1–5

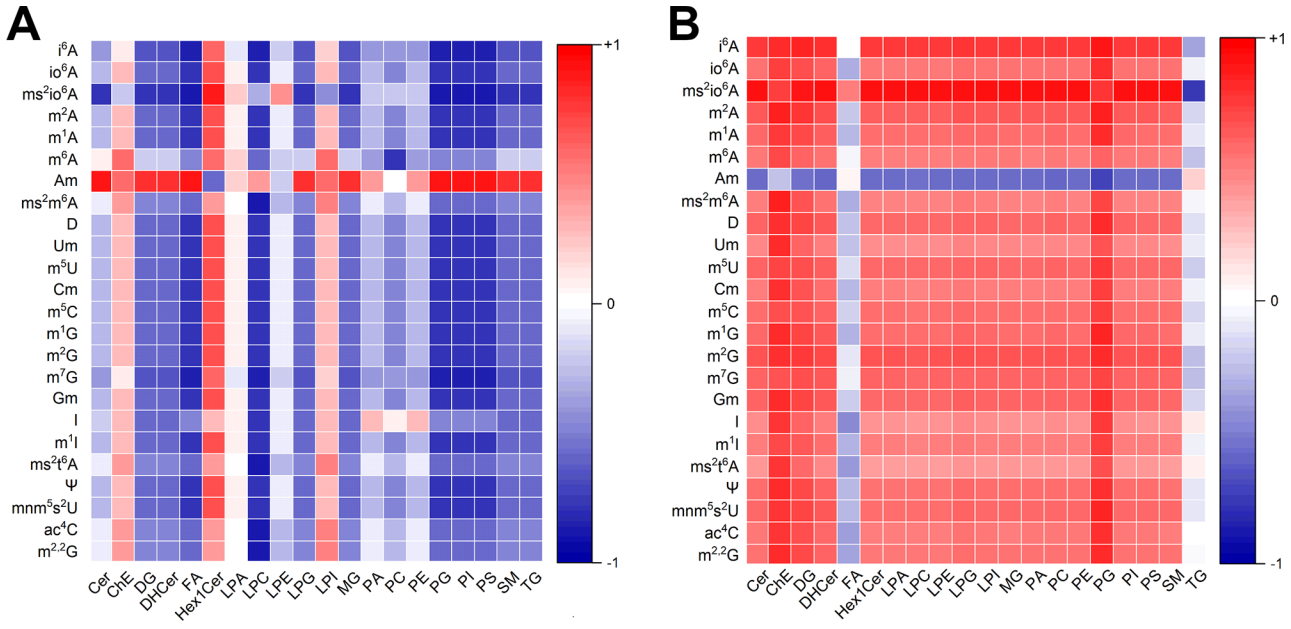

Fig. 8 Correlation analysis between tRNA modifications and lipids. Red represents a positive correlation, while blue represents a negative correlation. (**A**) Associations between the relative intensity of 24 types of tRNA modifications and the absolute content of 20 lipid classes throughout fruit development (Phase 1–5).; (**B**) Correlations between 24 tRNA modifications and the compositional ratios (amount of individual class / total lipid) of 20 lipid classes during fruit maturation (Phase 1–5)

We delved deeper into the relationship between tRNA modifications, fatty acids' saturation levels, and chain lengths within lipids. Our analysis revealed that fatty acids with either 0 or 6 double bonds tended to correlate positively with most tRNA modifications, except for Am, which exhibited a negative correlation (Fig. 9A). Interestingly, Am was the only tRNA modification with a positive correlation with fatty acids possessing 1–3 double bonds. This distinct behavior of Am was further validated through our analyses of DGs and TGs, depicted in Fig. 9A. In this context, ms^2io^6A again showed a contrasting stance to Am, yet its correlation patterns with tRNA modifications, apart from Am, were akin but more marked. This correlation between tRNA modifications and lipid saturation points to a nuanced connection, leading to our hypothesis that certain tRNA modifications might preferentially enhance the translation of specific enzymes involved in fatty acid desaturation. Figure 9B shows that specific tRNA modifications are associated with certain fatty acid chain lengths, highlighting the unique role of Am and its contrast with ms^2io^6A. Am showed a positive correlation with FAs containing 14, 18, and 20 carbons, DGs with 32 and 36 carbons, and TGs with longer carbon chains ranging from 51 to 58. Am correlated with fatty acid chains of specific lengths in FAs and DGs, as well as TGs with longer carbon chains. Interestingly, TGs with 48 and 52 carbons showed little correlation with tRNA modifications, suggesting they may be crucial lipids that require stable expression.

Conclusions

In this study, we used nucleoside and oligonucleotide analysis (RNA-MS), and gene comparison techniques to identify tRNA modifications and their modifying enzymes in oil palm for the first time. We also mapped their modification sites, including pseudouridine locations, enhancing our grasp of oil palm's basic biology. Our unique perspective investigated the dynamic changes in tRNA modifications and their correlation with lipid profiles during the development of oil palm fruits. Notably, tRNA modifications generally diminished throughout the fruit's maturation process, with a modest uptick in Phase 5, except for Am, which markedly increased during this stage. Contrary to other tRNA modifications, Am's association trends with certain lipid classes, carbon chain lengths, and saturation degrees, particularly against ms^2io^6A, suggest a divergent role. Considering ms^2io^6A's function as a cytokinin that encourages plant growth and limits energy storage, the function of Am in oil palm is also worthy of in-depth study. Our findings illuminate the dynamic nature of tRNA modifications during fruit development, underscoring their regulatory significance beyond mere maintenance roles.

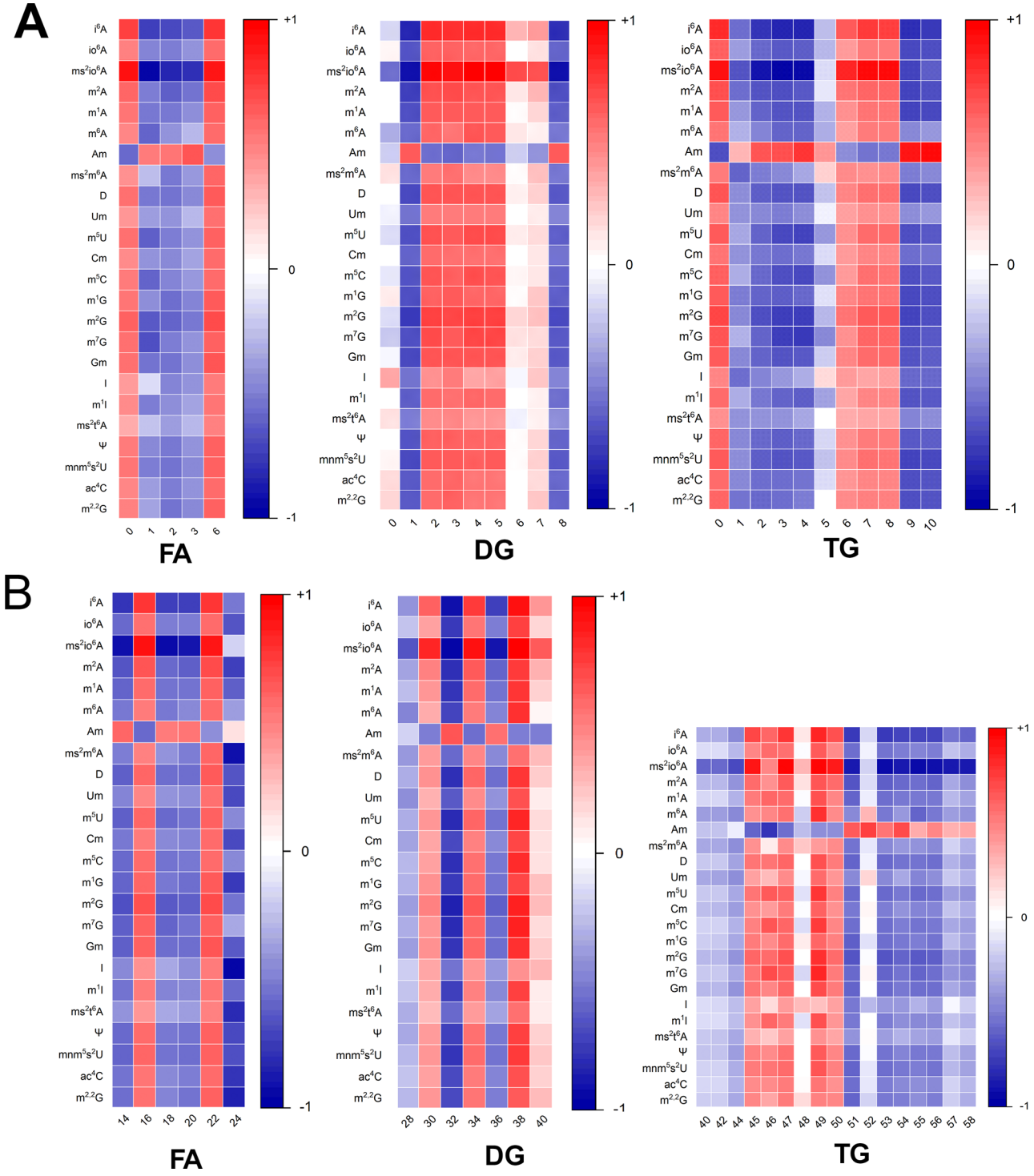

Fig. 9 The association between tRNA modifications and lipid fatty acid chain length and saturation status is analyzed. Red represents a positive correlation, while blue represents a negative correlation. (**A**) Correlation between the saturation level (number of double bonds) of fatty acid chains in FAs, DGs, and TGs and 24 tRNA modifications; (**B**) Association between the length of fatty acid chains in FAs, DGs, and TGs and tRNA modifications

Abbreviations

A	Adenosine
U	Uridine
C	Cytidine
G	Guanosine
I	Inosine
m^1I	1-methylinosine
m^1Im	1,2′-O-dimethylinosine
i^6A	N^6-isopentenyladenosine
io^6A	N^6-cis-hydroxyisopentenyladenosine
ms^2i^6A	2-methylthio-N^6-isopentenyladenosine
ms^2io^6A	2-methylthio-N^6-cis-hydroxyisopentenyladenosine

m^1A	1-methyladenosine
m^2A	2-methyladenosine
m^6A	N^6-methyladenosine
Am	2′-O-methyladenosine
ms^2m^6A	2-methylthio-N^6-methyladenosine
t^6A	N^6-threonylcarbamoyladenosine
ct^6A	cyclic N^6-threonylcarbamoyladenosine
ms^2t^6A	2-methylthio-N^6-threonylcarbamoyladenosine
Ar(p)	2′-O-ribosyladenosine (phosphate)
D	Dihydrouridine
Ψ	pseudouridine
Um	2′-O-methyluridine
m^5U	5-methyluridine
$mchm^5Um$	5-(carboxyhydroxymethyl)-2′-O-methyluridine methyl ester
cm^5U	5-carboxymethyluridine
cmo^5U	uridine 5-oxyacetic acid
mcm^5U	5-methoxycarbonylmethyluridine
$cmnm^5Um$	5-carboxymethylaminomethyl-2′-O-methyluridine
ncm^5U	5-carbamoylmethyluridine
mnm^5s^2U	5-methylaminomethyl-2-thiouridine
mcm^5s^2U	5-methoxycarbonylmethyl-2-thiouridine
ho^5U	5-hydroxyuridine
s^2U	2-thiouridine; acp3U:3-(3-amino-3-carboxypropyl)-uridine
Cm	2′-O-methylcytidine
ac^4C	N^4-acetylcytidine
ac^4Cm	N^4-acetyl-2′-O-methylcytidine
s^2C	2-thiocytidine
m^3C	3-methylcytidine
m^5C	5-methylcytidine
m^1G	N^1-methylguanosine
m^2G	N^2-methylguanosine
m^7G	7-methylguanosine
$m^{2,2}G$	N^2,N^2-methylguanosine
Gm	2′-O-methylguanosine
perQ1	7-aminomethyl-7-deazaguanosine
Q	Queuosine
imG-14	4-demethylwyosine
yW	wybutosine
yW-86	7-aminocarboxypropyl-demethylwyosine
yW-72	7-aminocarboxypropylwyosine
yW-58	7-aminocarboxypropylwyosine methyl ester
OHyW	hydroxywybutosine
Cer	Ceramide
ChE	Cholesteryl ester
DG	Diacylglycerol
DHCer	Dihydroceramide
FA	Fatty acids
Hex1Cer	monohexosylceramide
LPA	Lyso-phosphatidic acid
LPC	Lyso-phosphatidylcholine
LPE	Lyso-phosphatidylethanolamine
LPG	Lyso-phosphatidylglycerol
LPI	Lyso-phosphatidylinositol
MG	Monoglyceride
PA	Phosphatidic acid
PC	Phosphatidylcholine
PE	Phosphatidylethanolamine
PG	Phosphatidylglycerol
PI	Phosphatidylinositol
PS	Phosphatidylserine
SM	Sphingomyelin
TG	Triglyceride

Supplementary Information

The online version contains supplementary material available at https://doi.org/10.1186/s12870-025-06426-9.

Supplementary Material 1

Supplementary Material 2

Supplementary Material 3

Supplementary Material 4

Acknowledgements
We thank Jia Zhou of the Chinese academy of tropical agricultural sciences for her kind technical support.

Author contributions
DD, YQ, XL, and MC conducted experiments and contributed to data collection and analysis. DD interpreted data. DL, HL conceptualized this study. HL supervised the research. DD, HL wrote the manuscript. All authors reviewed the manuscript.

Funding
This study was funded by the Hainan Provincial Natural Science Foundation of China (Grant No. 2019RC003, 220MS004), and the National Natural Science Foundation of China (Grant No. 31900436, 42267067).

Data availability
Data will be made available upon reasonable request.

Declarations

Ethics approval and consent to participate
Not applicable.

Consent for publication
Not applicable.

Competing interests
The authors declare no competing interests.

Received: 14 March 2024 / Accepted: 19 March 2025
Published online: 29 March 2025

References

1. Loh SK. The potential of the Malaysian oil palm biomass as a renewable energy source. Energy Conv Manag. 2017;141:285–98.
2. Murphy D, Goggin K, Paterson R. Oil palm in the 2020s and beyond: challenges and solutions. CABI Agric Biosci. 2021;2(39):1–22.
3. Goggin KA, Murphy DJ. Monitoring the traceability, safety and authenticity of imported palm oils in Europe. OCL. 2018;25(6):A603.
4. Yue GH, Ye BQ, Lee M. Molecular approaches for improving oil palm for oil. Mol Breed. 2021;41(22):1–17.
5. Ithnin M, Kushairi A. The oil palm genome. Springer; 2020.
6. Corley RHV, Tinker PB. The oil palm. Fifth edn: Wiley; 2015.
7. Hoffmann MP, et al. Yield gap analysis in oil palm: framework development and application in commercial operations in Southeast Asia. Agric Syst. 2017;151:12–9.
8. Yue G, Ye B, Suwanto A. The unavoidable palm oil can be sustainable. Int J Oil Palm. 2020;3(2):29–39.
9. Rajanaidu N, Din AK, Din M. Monograph oil palm genetic resources. Malaysian Palm Oil Board. 2017.
10. Rohani O, et al. Mutation induction using gamma irradiation on oil palm (*Elaeis guineensis Jacq.*) cultures. J Oil Palm Res. 2012;24:1448–58.
11. Dunwell JM, et al. Production of haploids and doubled haploids in oil palm. BMC Plant Biol. 2010;10(218):1–25.
12. Parveez GKA, et al. Transgenic oil palm: production and projection. Portland. 2000.
13. Tisserat B. Clonal propagation of palms. In: Lindsey K, editor. Plant tissue culture manual: supplement 7. Springer; 1991. pp. 473–86.
14. Babu BK, et al. Development, identification and validation of CAPS marker for SHELL trait which governs Dura, pisifera and tenera fruit forms in oil palm (*Elaeis guineensis Jacq*). PLoS ONE. 2017;12(2):e0171933.
15. Yarra R, et al. CRISPR/Cas mediated base editing: a practical approach for genome editing in oil palm. 3 Biotech. 2020;10(306):1–7.

16. Uthaipaisanwong P, et al. Characterization of the Chloroplast genome sequence of oil palm (*Elaeis guineensis Jacq*). Gene. 2012;500(2):172–80.
17. Singh R, et al. Oil palm genome sequence reveals divergence of interfertile species in old and new worlds. Nature. 2013;500(7462):335–9.
18. Ong A-L, et al. An improved oil palm genome assembly as a valuable resource for crop improvement and comparative genomics in the Arecoideae subfamily. Plants. 2020;9(11):1476.
19. Wang L, et al. A Chromosome-level reference genome of African oil palm provides insights into its divergence and stress adaptation. Genomics Proteom Bioinf. 2023;21(3):440–54.
20. Dominissini D, et al. Topology of the human and mouse m^6A RNA methylomes revealed by m^6A-seq. Nature. 2012;485(7397):201–6.
21. Hartstock K, Rentmeister A. Mapping m^6A in RNA: established methods, remaining challenges and emerging approaches. Chemistry. 2019;25(14):3455–64.
22. Zhou J, et al. Dynamic m^6A mRNA methylation directs translational control of heat shock response. Nature. 2015;526(7574):591–4.
23. Boccaletto P, et al. MODOMICS: a database of RNA modification pathways. 2021 update. Nucleic Acids Res. 2022;50(D1):D231–5.
24. Suzuki T. The expanding world of tRNA modifications and their disease relevance. Nat Rev Mol Cell Biol. 2021;22(6):375–92.
25. Chionh YH, et al. tRNA-mediated codon-biased translation in mycobacterial hypoxic persistence. Nat Commun. 2016;7(13302):1–12.
26. Lin H, et al. CO_2-sensitive tRNA modification associated with human mitochondrial disease. Nat Commun. 2018;9:1875.
27. Lee WL, et al. An RNA modification enzyme directly senses reactive oxygen species for translational regulation in *Enterococcus faecalis*. Nat Commun. 2023;14:4093.
28. Chen P, Jäger G, Zheng B. Transfer RNA modifications and genes for modifying enzymes in *Arabidopsis Thaliana*. BMC Plant Biol. 2010;10(1):1–19.
29. Mehlgarten C, et al. Elongator function in tRNA wobble uridine modification is conserved between yeast and plants. Mol Microbiol. 2010;76(5):1082–94.
30. Zhou W, Karcher D, Bock R. Identification of enzymes for adenosine-to-inosine editing and discovery of cytidine-to-uridine editing in nucleus-encoded transfer RNAs of Arabidopsis. Plant Physiol. 2014;166(4):1985–97.
31. Wang Y, et al. The 2′-O-methyladenosine nucleoside modification gene OsTRM13 positively regulates salt stress tolerance in rice. J Exp Bot. 2017;68(7):1479–91.
32. Chu M, et al. A preliminary survey of transfer RNA modifications and modifying enzymes of the tropical plant *Cocos nucifera L*. Genes. 2023;14(6):1287.
33. Tranbarger TJ, et al. Regulatory mechanisms underlying oil palm fruit mesocarp maturation, ripening, and functional specialization in lipid and carotenoid metabolism. Plant Physiol. 2011;156(2):564–84.
34. Qin Y, et al. Micro-flow hydrophilic interaction liquid chromatography coupled with triple quadrupole mass spectrometry detects modified nucleosides in the transfer RNA pool of cyanobacteria. J Sep Sci. 2021;44(17):3208–18.
35. Su D, et al. Quantitative analysis of ribonucleoside modifications in tRNA by HPLC-coupled mass spectrometry. Nat Protoc. 2014;9(4):828–41.
36. Yang W-Q, et al. THUMPD3–TRMT112 is a m^2G methyltransferase working on a broad range of tRNA substrates. Nucleic Acids Res. 2021;49(20):11900–19.
37. Fu Y, et al. Degradation of lipid droplets by chimeric autophagy-tethering compounds. Cell Res. 2021;31(9):965–79.
38. Chao J, et al. MG2C: A user-friendly online tool for drawing genetic maps. Mol Hortic. 2021;1(16):1–4.
39. Chan PP, Lowe TM. tRNAscan-SE: searching for tRNA genes in genomic sequences. Methods Mol Biol. 2019;1962:1–14.
40. Yu N, et al. RNAModMapper: RNA modification mapping software for analysis of liquid chromatography tandem mass spectrometry data. Anal Chem. 2017;89(20):10744–52.
41. Giessing AM, Kirpekar F. Mass spectrometry in the biology of RNA and its modifications. J Proteom. 2012;75(12):3434–49.
42. Mengel-Jørgensen J, Kirpekar F. Detection of Pseudouridine and other modifications in tRNA by cyanoethylation and MALDI mass spectrometry. Nucleic Acids Res. 2002;30(23):e135–135.
43. Yu Q, et al. RNA demethylation increases the yield and biomass of rice and potato plants in field trials. Nat Biotechnol. 2021;39(12):1581–8.
44. Hou N, et al. MdMTA-mediated m^6A modification enhances drought tolerance by promoting mRNA stability and translation efficiency of genes involved in lignin deposition and oxidative stress. New Phytol. 2022;234(4):1294–314.
45. Torres AG, et al. A-to-I editing on tRNAs: biochemical, biological and evolutionary implications. FEBS Lett. 2014;588(23):4279–86.
46. Wilkinson ML, et al. The 2′-O-methyltransferase responsible for modification of yeast tRNA at position 4. RNA Biol. 2007;13(3):404–13.
47. Gibb M, et al. The origins and roles of methylthiolated cytokinins: evidence from among life kingdoms. Front Cell Dev Biol. 2020;8:605672.

Publisher's note